

## Research Article

# Dynamic Stability and Control of a Manipulating Unmanned Aerial Vehicle

Yunping Liu , Xijie Huang, Yonghong Zhang, and Yukang Zhou

*Jiangsu Collaborative Innovation Center of Atmospheric Environment and Equipment Technology (CICAEET), Nanjing University of Information Science & Technology, Nanjing 210044, China*

Correspondence should be addressed to Yunping Liu; liuyunping@nuist.edu.cn

Received 16 November 2017; Accepted 9 May 2018; Published 12 June 2018

Academic Editor: Paul Williams

Copyright © 2018 Yunping Liu et al. This is an open access article distributed under the Creative Commons Attribution License, which permits unrestricted use, distribution, and reproduction in any medium, provided the original work is properly cited.

This paper focuses on the dynamic stability analysis of a manipulator mounted on a quadrotor unmanned aerial vehicle, namely, a manipulating unmanned aerial vehicle (MUAV). Manipulator movements and environments interaction will extremely affect the dynamic stability of the MUAV system. So the dynamic stability analysis of the MUAV system is of paramount importance for safety and satisfactory performance. However, the applications of Lyapunov's stability theory to the MUAV system have been extremely limited, due to the lack of a constructive method available for deriving a Lyapunov function. Thus, Lyapunov exponent method and impedance control are introduced, and the Lyapunov exponent method can establish the quantitative relationships between the manipulator movements and the dynamics stability, while impedance control can reduce the impact of environmental interaction on system stability. Numerical simulation results have demonstrated the effectiveness of the proposed method.

## 1. Introduction

Unmanned aerial vehicles (UAVs), especially the quadrotors, have developed rapidly and been widely applied in many ways [1], for example, aerial photography, power line patrol, and surveillance [2]. However, these applications mentioned all avoid interacting with the environments. For some environmental interaction tasks, the active operation of UAVs endowed with manipulator will greatly expand their range of applications, while it brings great challenges in dynamic stability for the whole system. As is well known, UAVs have many stability problems, such as shaking, out of control, and even crash, and if endowed with manipulators, UAVs stability will additionally be affected by manipulator movements and environment contacts. So dynamic stability researches of UAVs especially MUAVs are very necessary and important to ensure that the whole system is safe and reliable.

The field of MUAVs is still largely an immature one, but it has received great concern and some recent attempts have been made. Earlier studies focused on the installation of a lightweight gripper at the belly of the aircraft [3–5]. The gripper has less impact on the UAV, but the operating ability is very limited,

so the later research mainly focused on changing the gripper device into a manipulator [6–9]. Manipulator, especially redundant manipulator, has flexible operation [10, 11]. However, manipulator movements and the environment contact will change the center of gravity position and reduce system stability [12]. On theoretical research, Euler Lagrange [13–15] and Newton-Euler [16–18] methods have been widely used to establish the dynamics model. But complex computation always brings great difficulties to model derivation.

As for nonlinear system stability analysis, the most commonly used method is Lyapunov's stability theory [19–21]. It plays a very important role in the system stability proof and the controller design, and Lyapunov functions are needed when using this method. However, there is no constructive method available for deriving the functions, so it is quite difficult to establish the Lyapunov functions especially for the nonlinear system of MUAV with multiple variables, strong coupling, and underactuation. To solve this problem, Lyapunov exponent method has been introduced and widely used. Lyapunov exponents are the average exponential rates of divergence or convergence of nearby orbits in the state space, and they are related to the expanding or contracting

nature of different directions in the  $n$ -dimensional phase space of a continuous dynamical system [22]. The concept of Lyapunov exponents provides a generalization of the linear stability analysis for perturbations of steady-state solutions to time-dependent solutions [23, 24]. Yang and Wu and Sun and Wu [25, 26] applied Lyapunov exponent method to study the dynamic stability of bipedal robots during disturbed standing. Abdulwahab et al. [27] used Lyapunov exponent method to analyze the lateral flight stability of unmanned aerial vehicles. In our previous work [28], quantitative relationship between the structural parameters of a quadrotor and the dynamic stability was established based on the Lyapunov exponent. By optimizing the different structural parameters, we improved the quadrotor dynamic stability. Since MUAVs usually need to interact with the environment, it is necessary to take some measures to ensure the stability of the system and avoid damage to the devices. Bartelds et al. [29] designed a compliant mechanism to allow the aerial manipulator to remain stable during and after impact. Alexis et al. [30] proposed a hybrid model predictive control framework to ensure the quadrotor stable and active interaction. In [31], impedance control was introduced to deal with the interaction between the end effector mounted on a ducted fan UAV and a vertical wall.

This paper focuses on the modeling and the dynamic stability analysis of a single DOF manipulator mounted on a quadrotor unmanned aerial vehicle. The Euler-Poincare equations are introduced to derive kinematics and dynamics model of the MUAV system. As for dynamic stability, the manipulator movements and the environmental interactions are considered separately. Lyapunov exponent method is used to analyze the stability affected by different manipulator movements and then the Newton-Euler recursive method is used to quantify the coupling between the manipulator and the quadrotor, after which coupling compensation is considered in the controller design. In order to ensure stability and safety when the end effector of the manipulator interacts with the environment, an impedance controller is designed. Numerical simulations illustrate the effectiveness of the controller in the force-constrained space as well as the transition from the free space to the force-constrained space.

The rest of this paper is organized as follows. Section 2 presents the overall system model. In Section 3, dynamics stability and coupling characteristics of the system due to manipulator movements are analyzed. In Section 4, the complete interaction control architecture is proposed, and its effectiveness is demonstrated in Section 5 by means of numerical simulation. Finally, some conclusions are presented in Section 6.

## 2. System Modeling

The system considered in this paper, depicted in Figure 1, is composed of a quadrotor vehicle equipped with a single DOF manipulator. One end of the manipulator is mounted at the geometric center of the four quadrotors (assuming that the geometric center coincides with the center of mass of the quadrotor).

To facilitate modeling, let  $\Sigma : E - XYZ$  be the inertial frame, and  $\Sigma_b : B - xyz$  is the UAV body frame with origin

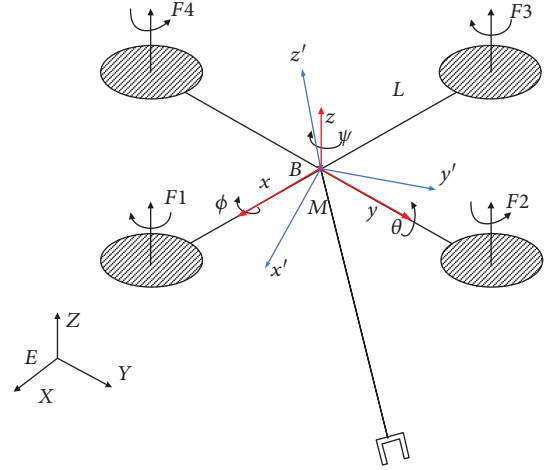


FIGURE 1: Quadrotor and manipulator system with the corresponding frames.

at the vehicle center of mass.  $\Sigma_m : M - x'y'z'$  is a manipulator frame, whose origin coincides with  $\Sigma_b$ , and the  $z'$  axis is in the direction of the reverse extension line of the manipulator. The configuration of the MUAV system can be given by

$$\mathbf{q} = [\boldsymbol{\eta}_u^T \quad \mathbf{p}_u^T \quad a]^T, \quad (1)$$

where  $\boldsymbol{\eta}_u = [\psi \quad \theta \quad \phi]^T$  denotes the quadrotor attitude, and vector  $\mathbf{p}_u = [x \quad y \quad z]^T$  is the position of the quadrotor with respect to  $\Sigma$ , and  $a$  is the joint angle of the manipulator. It is obvious that  $\mathbf{q}$  is the generalized coordinate of the MUAV system. Relative to  $\mathbf{q}$ , the pseudovelocity vector of the system can be given by

$$\mathbf{p} = [\boldsymbol{\omega}_u^T \quad \mathbf{v}_u^T \quad b]^T, \quad (2)$$

where  $\mathbf{v}_u = [u \quad v \quad w]^T$  and  $\boldsymbol{\omega}_u = [p \quad q \quad r]^T$ , respectively, denote linear velocity and angular velocity component of the quadrotor in  $\Sigma_b$ , and  $b$  is the joint angular velocity of the manipulator.

The position of the end effector in  $\Sigma$  is represented as

$$\mathbf{p}_e = \mathbf{p}_u + \mathbf{R}_u \mathbf{p}_e^b, \quad (3)$$

where  $\mathbf{R}_u$  is the rotation matrix of the  $\Sigma_b$  relative to  $\Sigma$ .  $\mathbf{p}_e^b$  is the position of the end effector in  $\Sigma_b$  and  $\mathbf{p}_e^b = [x_e^b \quad y_e^b \quad z_e^b]^T$ . Some symbols and descriptions are as follows:

$m_1$ : Mass of the quadrotor vehicle

$m_2$ : Mass of the manipulator

$g$ : Local gravity acceleration

$L$ : Length of the quadrotor from the center of mass to rotor axis

$R_Q$ : Rotor radius

$R$ : Length of the manipulator from the root to the center of mass

$S$ : Length of the manipulator

$C_Q$ : Coefficient of the rotor torque

$C_T$ : Rotor tensile force coefficient

$\rho$ : Local air density

$I_x, I_y,$  and  $I_z$ : Quadrotor moment of inertia of axis  $x, y,$  and  $z$

$J_y$ : Moment of inertia of the manipulator link about its center of mass

$w_i$ :  $i$ th rotor speed.

The MUAUV system is composed of two single rigid bodies, the quadrotor, and the manipulator. The quadrotor has 6 degrees of freedom, and the manipulator has 1 degree of freedom rotating around the  $y$ -axis of  $\sum_b$ . The kinematics and dynamics equations of MUAUV based on Euler-Poincare equations (5) can be derived with the Mathematica software package TSI ProPac [32]. The modeling process is as follows:

(i) Define joint data:

```
r1 = {6}; H1 = IdentityMatrix [6];
q1 = {phi, theta, psi, x, y, z}; p1 = {p, q, r, u, v, w};
r2 = {1}; H2 = {{0}, {1}, {0}, {0}, {0}, {0}};
q2 = {a}; p2 = {b};
JointLst = {{r1, H1, q1, p1}, {r2, H2, q2, p2}};
```

(ii) Define body data:

```
com1 = {0, 0, 0}; mass1 = m1; out1 = {2, {0, 0, 0}};
Inertia1 = {{Ix, 0, 0}, {0, Iy, 0}, {0, 0, Iz}};
com2 = {0, 0, -R}; mass2 = m2; out2 = {3, {0, 0, -S}};
Inertia2 = {{0, 0, 0}, {0, Jy, 0}, {0, 0, 0}};
BodyLst = {{com1, {out1}, mass1, Inertia1}, {com2, {out2}, mass2, Inertia2}};
```

(iii) Define interconnection structure:

```
TreeLst = {{{1, 1}, {2, 2}}};
```

(iv) Define potential energy and nonconservative generalized input force/torque:

```
PE = 0;
T1 = U2; T2 = U3; T3 = U4;
Q = {T1, T2, T3, 0, 0, U1, T4};
```

(v) Modeling.

```
{JV, JX, JH, MM, Cp, Fp, pp, qq} = CreateModel
[JointLst, BodyLst, TreeLst, g, PE, Q, JV, JX, JH];
```

```
Equations = MakeODEs [pp, qq, JV, MM, Cp, Fp, t]
```

where  $U_1, U_2, U_3,$  and  $U_4$  are the control inputs of vertical height, roll angle, pitching angle, and yawing angle, respectively, and

$$\begin{aligned} U_1 &= F_1 + F_2 + F_3 + F_4, \\ U_2 &= F_2 - F_4, \\ U_3 &= F_3 - F_1, \\ U_4 &= F_1 - F_2 + F_3 - F_4, \end{aligned} \quad (4)$$

where  $F_i$  ( $i = 1, \dots, 4$ ) is the lift of the  $i$ th rotor. If we define  $A = \pi R_q^2$ , then the thrust of each rotor can be expressed as  $F_i = 1/2 \rho A C_T R_q^2 \omega_i^2$ . The main matrix parameters can be obtained through the above symbolic calculation. With these matrix parameters, the MUAUV system model can be finally obtained in the form of

$$\begin{aligned} \dot{\mathbf{q}} &= \mathbf{V}(\mathbf{q})\mathbf{p}, \\ \mathbf{M}(\mathbf{q})\dot{\mathbf{p}} + \mathbf{C}(\mathbf{q}, \mathbf{p})\mathbf{p} + \mathbf{F}(\mathbf{p}, \mathbf{q}, \mathbf{u}) &= \mathbf{0}, \end{aligned} \quad (5)$$

where  $\mathbf{V}(\mathbf{q})$ ,  $\mathbf{M}(\mathbf{q})$ , and  $\mathbf{C}(\mathbf{q}, \mathbf{p})$  are kinematics matrix, inertia matrix, and gyroscopic matrix, respectively.  $\mathbf{F}(\mathbf{p}, \mathbf{q}, \mathbf{u})$  is the viscous friction and gravity vector.

### 3. Dynamic Stability Analysis

The quadrotor, as the base of the manipulator, is different from the traditional fixed base and it is essentially unstable. However, a stable base is really required when the manipulator performs some operation. Thus, the dynamic analysis of a system is quite important. Considering the limitations of the Lyapunov's stability theory for complicated nonlinear systems, in this section, Lyapunov exponent method is applied to analyze the dynamic stability of the MUAUV system in the case of manipulator movements. As is well known, when it comes to stability analysis, Lyapunov exponents are usually compared with 0, and some relationships between Lyapunov exponents and system stability can be concluded. If all Lyapunov exponents are less than zero, the system is exponentially stable about the equilibrium point, which indicates that the system is dissipative or nonconservative. On the contrary, when at least one Lyapunov exponent is greater than zero; the system tends to be unstable or chaotic. And if the value of Lyapunov exponents is fixed at zero, the phase trajectory is periodic with time [33]. Lyapunov exponent can be applied to establish the quantitative relationships between the manipulator movements and the MUAUV dynamic stability. The Lyapunov exponent calculation is based on the established mathematical model of the MUAUV. Different manipulators movements lead to the kinematics and dynamics model of the MUAUV different, which indicates that the corresponding Lyapunov exponent may change. Lyapunov exponent can be calculated as

$$\lambda = \lim_{n \rightarrow \infty} \frac{1}{n} \sum_{i=0}^{n-1} \ln \left| \frac{df(\mathbf{X})}{d\mathbf{X}} \right|_{X_i}, \quad (6)$$

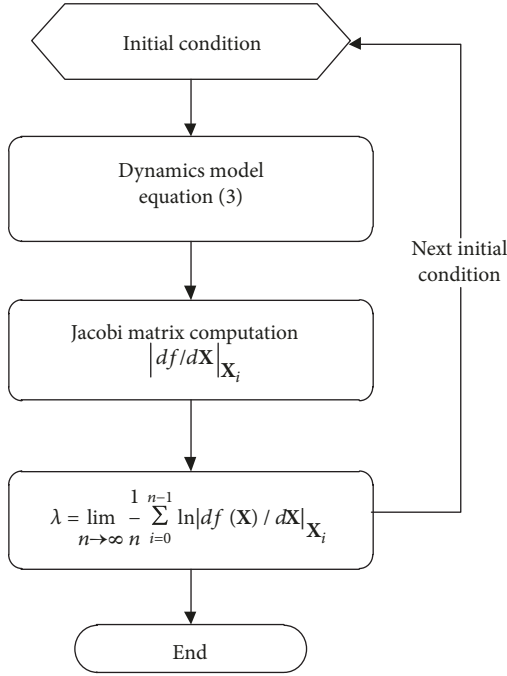


FIGURE 2: Calculation process of the Lyapunov exponent.

where  $df(\mathbf{X})/d\mathbf{X}$  is Jacoby matrix of the system, and  $n$  is the number of iterations. In order to compute the Jacoby matrix, (5) needs to be translated into

$$\begin{aligned} \dot{\mathbf{q}} &= \mathbf{V}(\mathbf{q})\mathbf{p}, \\ \dot{\mathbf{p}} &= -\mathbf{M}^{-1} \cdot (\mathbf{C} \cdot \mathbf{p} + \mathbf{F}). \end{aligned} \quad (7)$$

Let

$$\dot{\mathbf{X}} = [\mathbf{q}, \mathbf{p}]^T = [\phi, \theta, \psi, x, y, z, a, p, q, r, u, v, w, b]^T, \quad (8)$$

and (7) can be reformulated as

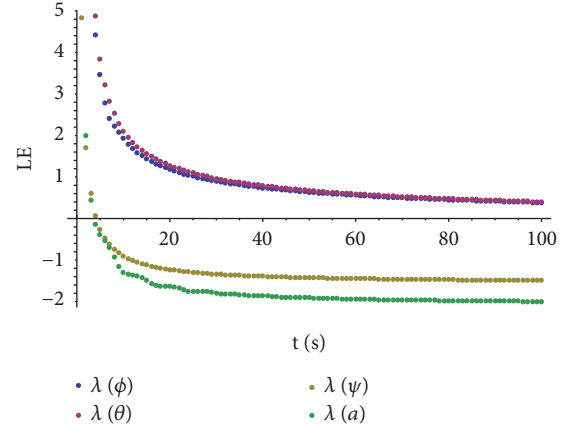
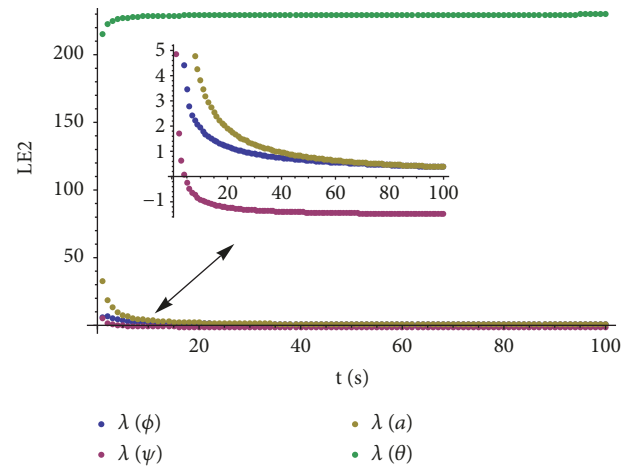
$$\dot{\mathbf{X}} = \mathbf{f}(\mathbf{X}, \mathbf{u}), \quad (9)$$

where  $\mathbf{u}$  is control input vector. Figure 2 displays the specific calculation process.

When designing manipulator controller with different expected manipulator joint angle, the joint torque T4 in step (iv) of the MUAV dynamic modeling changes, which makes the dynamic model changes as well. Then, the calculated Lyapunov exponents will also be different based on Figure 2 and after  $n$  iteration, the trajectory distance between the disturbed MUAV system and the original system is as follows:

$$\lim_{n \rightarrow \infty} \varepsilon \cdot e^{n\lambda(x_0)} = \lim_{n \rightarrow \infty} |f^n(x_0 + \varepsilon) - f^n(x_0)|. \quad (10)$$

It can be known that if  $\lambda > 0$ ,  $\lim_{n \rightarrow \infty} \varepsilon \cdot e^{n\lambda} \rightarrow \infty$  will tend to infinity, which shows that the disturbed trajectory and the original trajectory of the system is separated with time and the system is chaotic, and if  $\lambda < 0$ ,  $\lim_{n \rightarrow \infty} \varepsilon \cdot e^{n\lambda} \rightarrow 0$  will tend to zero, which illustrates that after disturbed, the system can reach the original system state again and the system is insensitive to the disturbance and stable.

FIGURE 3: Lyapunov exponents spectrum of the MUAV ( $a_d=0$ ).FIGURE 4: Lyapunov exponents spectrum of the MUAV ( $a_d=\sin a$ ).

According to the method described above, when the quadrotor is hovering, Lyapunov exponents of the system are calculated separately with different manipulator movements. When setting the number of iterations to 100 and the initial state ( $[\mathbf{q}, \mathbf{p}]^T$ ) of the MUAV system to  $[0, 0, 0, 0, 0, 0, 0, 0, 0, 0, 0, 0, 0, 0]^T$ , the Lyapunov exponents of the system can be obtained. For a clear analysis, Lyapunov exponents of the quadrotor attitudes and manipulator joint angle are shown in Figures 3 and 4. When the desired joint angle  $a_d$  of the manipulator is 0, that is, the quadrotor and the manipulator are relative stationary, the Lyapunov exponents spectrum is shown in Figure 3. Similarly, set  $a_d = \sin a$ , then the Lyapunov exponents spectrum of the quadrotor attitudes and manipulator joint angle are shown in Figure 4.

From Figures 3 and 4, we can see that the Lyapunov exponents of Figure 3 are less than 0 or tend to be 0, while in Figure 4, there is one exponent that is greater than 200 with no tendency to 0. In comparison with these two figures, when there is relative motion between the manipulator and the quadrotor, the dynamic stability of the whole system is obviously getting worse; in severe cases, the whole system may get unstable.

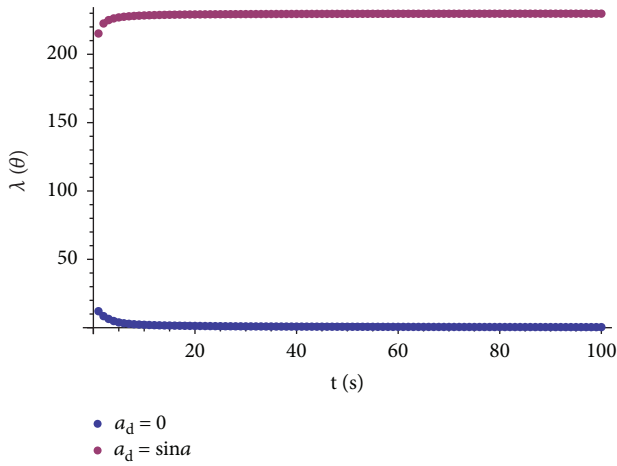


FIGURE 5: Lyapunov exponents of the pitch angles under two conditions.

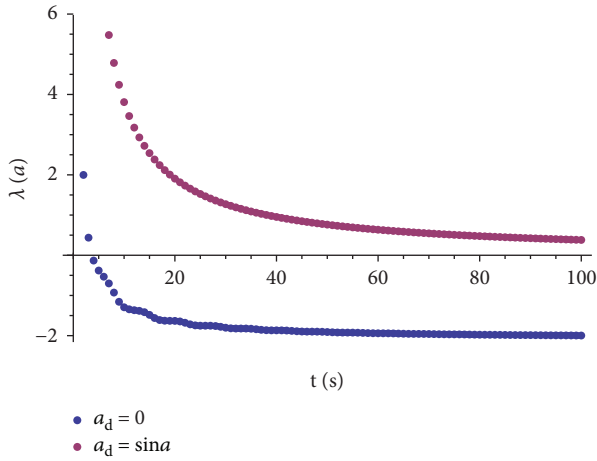


FIGURE 6: Lyapunov exponents of the joint angles under two conditions.

From Figures 3 and 4, it can be seen that the Lyapunov exponents of the corresponding roll angle and yaw angle are almost the same while the Lyapunov exponents of the corresponding pitch angle and manipulator joint angle differ. For a clearer analysis, the Lyapunov exponents of pitch angles and joint angles are shown in Figures 5 and 6.

Figure 5 shows that the Lyapunov exponent of the pitch angle in the condition of  $a_d = \sin a$  is much larger than that of  $a_d = 0$ , which indicates that the dynamic stability gets worse when the manipulator movements exist and the manipulator movements will affect the quadrotor pitching motion, and even may lead to the instability.

According to Figure 6, the joint angle Lyapunov exponent is less than 0 when  $a_d = 0$ . However, the exponent changes when  $a_d = \sin a$ , that is, relative motion between the robot arm and the quadrotor presents, which indicates that manipulator motion, in turn, is affected by the quadrotor motion.

From Figures 5 and 6, it can be concluded that the quadrotor pitching motion and the manipulator motion are coupled. This coupling characteristic will have very bad effects on the subsequent control and practical applications, so it is

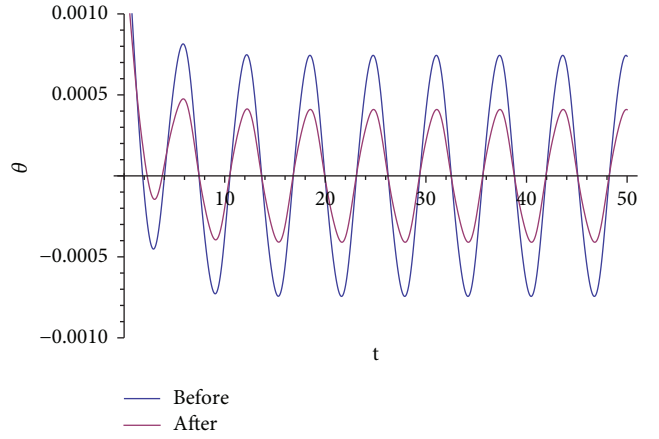


FIGURE 7: Pitch angle simulation with/without coupling compensation.

necessary to analyze and quantify the coupling and then in the controller design, coupling, and compensation is needed.

Similar to the space manipulator [34], Newton-Euler recursive method [35] is used to quantify the coupling. Suppose that the quadrotor is the root of the manipulator, which can be thought link 0 and from the root to the end effector, the linear velocity, angular velocity, and acceleration of each link can be calculated. With velocity and acceleration, the force and torque on each link are derived backwards. Finally, the force applied on the quadrotor due to the manipulator movements can be calculated, and the derivation process is as follows.

For simplicity, some symbols are defined. Let  ${}^j\boldsymbol{\omega}_i$  and  ${}^j\mathbf{v}_i$  denote the angular velocity and the linear velocity of link  $i$  with respect to the link frame  $\Sigma_j$ .  $\alpha_i$  denotes the joint angle of link  $i$ .  $\dot{\alpha}_i$  represents the derivative of time.  ${}^j_i\mathbf{R}$  is the rotation matrix of the  $\Sigma_i$  relative to  $\Sigma_j$ .  ${}^j\mathbf{p}_i$  is the position of the  $i$ th joint in  $\Sigma_j$ , and  ${}^j\mathbf{h}_i$  represents the axis of rotation of link  $i$  in  $\Sigma_j$ .

From the root to the end effector, the angular velocity and linear velocity of each link at the origin of link frame can be calculated as follows:

$$\begin{aligned} {}^{k+1}\boldsymbol{\omega}_{k+1} &= {}^{k+1}_k\mathbf{R}^k\boldsymbol{\omega}_k + \dot{\alpha}_{k+1} {}^{k+1}\mathbf{h}_{k+1}, \\ {}^{k+1}\mathbf{v}_{k+1} &= {}^{k+1}_k\mathbf{R} \left( {}^k\mathbf{v}_k + {}^k\boldsymbol{\omega}_k \times {}^k\mathbf{p}_{k+1} \right), \end{aligned} \quad (11)$$

and on the time derivative, the corresponding acceleration can be obtained.

$$\begin{aligned} {}^{k+1}\dot{\boldsymbol{\omega}}_{k+1} &= {}^{k+1}_k\mathbf{R}^k\dot{\boldsymbol{\omega}}_k + {}^{k+1}_k\dot{\mathbf{R}}^k\boldsymbol{\omega}_k + \ddot{\alpha}_{k+1} {}^{k+1}\mathbf{h}_{k+1} \\ &= {}^{k+1}_k\mathbf{R}^k\dot{\boldsymbol{\omega}}_k + \ddot{\alpha}_{k+1} {}^{k+1}\mathbf{h}_{k+1} \times \left( {}^{k+1}_k\mathbf{R}^k\boldsymbol{\omega}_k \right) \\ &\quad + \ddot{\alpha}_{k+1} {}^{k+1}\mathbf{h}_{k+1}, \quad {}^{k+1}\dot{\mathbf{v}}_{k+1} \\ &= {}^{k+1}_k\mathbf{R} \left( {}^k\dot{\mathbf{v}}_k + {}^k\dot{\boldsymbol{\omega}}_k \times {}^k\mathbf{p}_{k+1} + {}^k\boldsymbol{\omega}_k \times {}^k\dot{\mathbf{p}}_{k+1} \right) \\ &= {}^{k+1}_k\mathbf{R} \left[ {}^k\dot{\mathbf{v}}_k + {}^k\dot{\boldsymbol{\omega}}_k \times {}^k\mathbf{p}_{k+1} + {}^k\boldsymbol{\omega}_k \times \left( {}^k\boldsymbol{\omega}_k \times {}^k\mathbf{p}_{k+1} \right) \right]. \end{aligned} \quad (12)$$

Let subscript  $c$  represent the center of mass of the link. Then, the linear velocity and acceleration of the link at the center of mass can be calculated as

$$\begin{aligned} {}^{k+1}\mathbf{v}_{c_{k+1}} &= {}^{k+1}\mathbf{v}_{k+1} + {}^{k+1}\boldsymbol{\omega}_{k+1} \times {}^{k+1}\mathbf{p}_{c_{k+1}}, \\ {}^{k+1}\dot{\mathbf{v}}_{c_{k+1}} &= {}^{k+1}\dot{\mathbf{v}}_{k+1} + {}^{k+1}\dot{\boldsymbol{\omega}}_{k+1} \times {}^{k+1}\mathbf{p}_{c_{k+1}} + {}^{k+1}\boldsymbol{\omega}_{k+1} \\ &\quad \times \left( {}^{k+1}\boldsymbol{\omega}_{k+1} \times {}^{k+1}\mathbf{p}_{c_{k+1}} \right). \end{aligned} \quad (13)$$

With the above velocity and acceleration, the generalized force  $\mathbf{F}$  and torque  $\mathbf{N}$  on each link at the center of

mass can be obtained from the end effector to the root as follows:

$$\begin{aligned} {}^{k+1}\mathbf{F}_{k+1} &= m_{k+1} {}^{k+1}\dot{\mathbf{v}}_{c_{k+1}}, \\ {}^{k+1}\mathbf{N}_{k+1} &= {}^{c_{k+1}}\mathbf{I}_{k+1} {}^{k+1}\dot{\boldsymbol{\omega}}_{k+1} + {}^{k+1}\boldsymbol{\omega}_{k+1} \times \left( {}^{c_{k+1}}\mathbf{I}_{k+1} {}^{k+1}\boldsymbol{\omega}_{k+1} \right), \end{aligned} \quad (14)$$

where  $m_{k+1}$  is the mass of link  $k+1$  and  ${}^{c_{k+1}}\mathbf{I}_{k+1}$  is the moment of inertia about the center of mass of link  $k+1$ . Then, the generalized force  $\mathbf{f}$  and torque  $\mathbf{n}$  on each link at the origin of link frame can be obtained as

$$\begin{aligned} {}^k\mathbf{f}_k &= \begin{cases} {}^k\mathbf{F}_k + {}^{k+1}\mathbf{R}^{k+1} \mathbf{f}_{k+1} & (k < n), \\ {}^k\mathbf{F}_k & (k = n), \end{cases} \\ {}^k\mathbf{n}_k &= \begin{cases} {}^k\mathbf{N}_k + {}^{k+1}\mathbf{R}^{k+1} \mathbf{n}_{k+1} + {}^k\mathbf{p}_{c_k} \times {}^k\mathbf{F}_k + {}^k\mathbf{p}_{k+1} \times \left( {}^{k+1}\mathbf{R}^{k+1} \mathbf{f}_{k+1} \right) & (k < n), \\ {}^k\mathbf{N}_k + {}^k\mathbf{p}_{c_k} \times {}^k\mathbf{F}_k & (k = n), \end{cases} \end{aligned} \quad (15)$$

where  $n$  is the number of the links.

The force and torque acting on the joint 1 can be obtained by recursive calculation, and they will be transmitted to the quadrotor. Thus, considering only the generalized force and torque exerted by the manipulator, the coupling between the manipulator and the quadrotor can be finally quantified as

$$\begin{aligned} {}^0\mathbf{F}_0 &= {}^0\mathbf{R}^1 \mathbf{f}_1, \\ {}^0\mathbf{N}_0 &= {}^0\mathbf{p}_1 \times ({}^0\mathbf{R}^1 \mathbf{f}_1) + {}^0\mathbf{R}^1 \mathbf{n}_1. \end{aligned} \quad (16)$$

In order to verify the quantized coupling, firstly, simple PID controllers are designed to control attitude and height of quadrotor and joint angle of the manipulator. Then, PID controllers with regard to coupling compensation are also applied to control the quadrotor and the manipulator. For the two cases, the pitch angle simulation is presented in Figure 7.

From Figure 7, the coupling exists both with and without feed-forward compensation. However, after compensation, the amplitude of the pitch angle oscillation is significantly decreased. Therefore, quantized coupling, when applied to control compensation, can play a certain role in controller design.

#### 4. Control Scheme

Compared with a conventional quadrotor, the aerial manipulator has the advantage of maneuverability. It can interact with the environments actively and perform some tasks. However, if the interaction force is too large, it is very likely to damage both the end effector and the objects. Also, the system may get unstable during the transition from free

motion to interaction. Thus, it is necessary to control the interaction force effectively. In this section, impedance control is adopted to solve the problem. Impedance control shows the dynamic relationship between interaction force and position [36]. In the Cartesian space, the desired impedance model of the end effector can be given by

$$\mathbf{M}_d(\ddot{\mathbf{X}}_d - \ddot{\mathbf{X}}) + \mathbf{B}_d(\dot{\mathbf{X}}_d - \dot{\mathbf{X}}) + \mathbf{K}_d(\mathbf{X}_d - \mathbf{X}) = \mathbf{F}_e, \quad (17)$$

where  $\mathbf{M}_d$ ,  $\mathbf{B}_d$ , and  $\mathbf{K}_d$  are the constant matrices of desired inertia, damping coefficient, and spring stiffness of the end effector. Vectors  $\mathbf{X}$  and  $\mathbf{X}_d$  are the actual and desired end effector position, respectively, and  $\mathbf{F}_e$  represents the generalized force exerted upon the end effector by the environment. By modeling interaction surface of the environment as a spring, the force  $\mathbf{F}_e$  can be calculated as

$$\mathbf{F}_e = \begin{cases} k_e(\mathbf{X}_{\text{env}} - \mathbf{X}) & \text{if } \mathbf{X} > \mathbf{X}_{\text{env}}, \\ 0 & \text{if } \mathbf{X} \leq \mathbf{X}_{\text{env}}, \end{cases} \quad (18)$$

where  $k_e$  is the stiffness of the environment while  $\mathbf{X}_{\text{env}}$  is the position of the interaction surface. When the interaction force arises, the corresponding torque applied to the manipulator is shown by

$$\mathbf{T}_e = \mathbf{J}^T \mathbf{F}_e, \quad (19)$$

where  $\mathbf{J}$  is the Jacoby matrix of the manipulator. Let  $\mathbf{e} = \mathbf{X}_d - \mathbf{X}$  represent the position error of the manipulator end effector and then convert (17) into frequency domain, it can be obtained as

$$\frac{\mathbf{F}_e(s)}{\mathbf{e}(s)} = \mathbf{M}_d s^2 + \mathbf{B}_d s + \mathbf{K}_d. \quad (20)$$

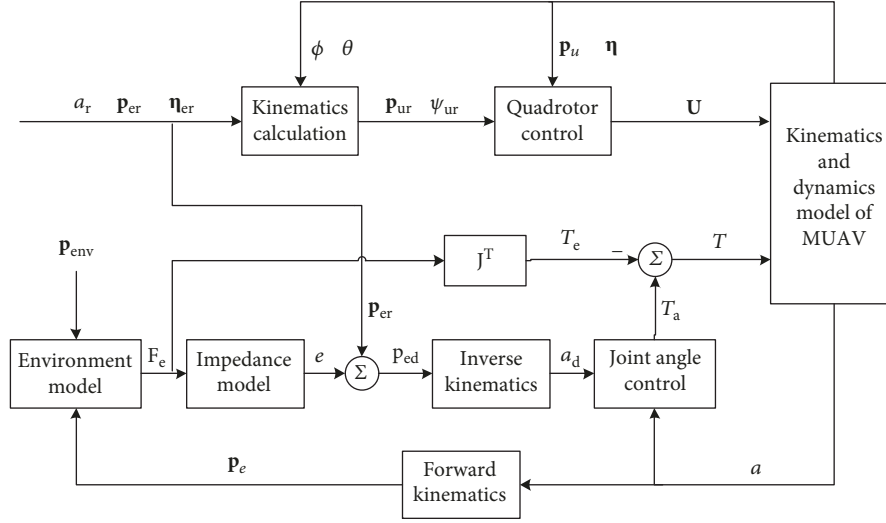


FIGURE 8: The impedance control block diagram.

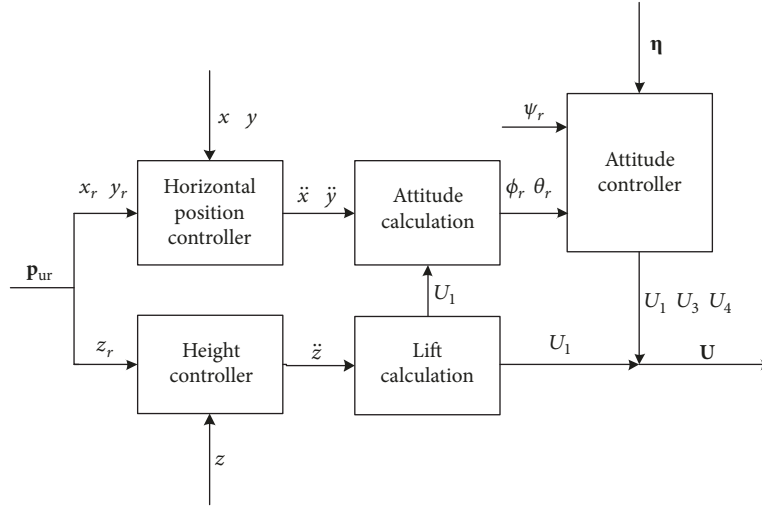


FIGURE 9: The quadrotor control block diagram.

Equation (20) can be changed into

$$\mathbf{e}(s) = \frac{\mathbf{F}(s)}{\mathbf{M}_d s^2 + \mathbf{B}_d s + \mathbf{K}_d}, \quad (21)$$

where  $\mathbf{e}$  is the position correction of the end effector. Summing it and the given reference position, the desired position of the end effector can be finally obtained. In the joint space, a PID controller applied to obtain the torque for the manipulator without regard to environmental interactions has the form:

$$T_a = k_p(a_d - a) + k_i \int (a_d - a) dt + k_d(\dot{a}_d - \dot{a}), \quad (22)$$

where  $k_p$ ,  $k_i$ , and  $k_d$  are the proportional, integral, and derivative control coefficients, respectively.  $a_d$  obtained through the inverse kinematics and  $a$  are the desired and actual joint

angles of the manipulator. If considering interactions, the actual torque can be given by

$$T = T_a - T_e. \quad (23)$$

As is shown in the impedance control block diagram in Figure 8, for the manipulator, a position-based impedance control (PBIC) is introduced and it includes a double control loop. The inner loop is position control and the outer loop is impedance control. According to the actual interaction force and desired impedance parameters, the outer loop generates position correction as represented in (21). When giving the reference position  $\mathbf{p}_{er}$ , attitude  $\boldsymbol{\eta}_{er}$  and joint angle  $a_r$  of the end effector as well as the feedback roll and pitch angle, the reference position  $\mathbf{p}_{ur}$ , and yaw angle  $\psi_r$  of the quadrotor can be obtained via a kinematics calculation algorithm proposed by [37]. Then with reference and the feedback position  $\mathbf{p}_u$  and attitude  $\boldsymbol{\eta}$  of the quadrotor, the quadrotor controller can be designed.

TABLE 1: MUAV parameters.

Symbols	Values
$m_1$	0.875 kg
$m_2$	0.106 kg
$g$	9.8 m/s <sup>2</sup>
$L$	0.225 m
$R$	0.1 m
$S$	0.2 m
$C_T$	$1.0792^{-005}$
$C_Q$	$1.8992^{-007}$
$R_q$	0.125 m
$\rho$	11.69 kg/m <sup>3</sup>
$I_x$	$9.5065^{-003}$ kg/m <sup>2</sup>
$I_y$	$1.00^{-002}$ kg/m <sup>2</sup>
$I_z$	$1.658^{-002}$ kg/m <sup>2</sup>
$J_y$	$2.37^{-003}$ kg/m <sup>2</sup>

For the quadrotor control shown in Figure 8, we can detail it as Figure 9 and it shows that a double PID control loop is also introduced. Since a quadrotor is underactuated, the horizontal position cannot be controlled directly with input forces. However, relationships between the horizontal acceleration and the reference attitude angles can be given by (24), where  $\ddot{x}, \ddot{y}$  denote the acceleration in  $x$  and  $y$  directions and subscript  $r$  represents the meaning of reference. Then, the double PID control loop can be designed with the inner loop being UAV attitude controller and the outer loop being UAV position controller, which ensures both position and attitude of the quadrotor reach expected states. When manipulator moves or makes contact with the environment, the controller also ensures UAV stability and even spot hover.

$$\begin{aligned} \phi_r &= \arcsin \left[ \frac{m_1 + m_2}{U_1} (\ddot{x} \sin \psi_r - \ddot{y} \cos \psi_r) \right], \\ \theta_r &= \arcsin \frac{(m_1 + m_2 / U_1) \ddot{x} - \sin \phi_r \sin \psi_r}{\cos \phi_r \cos \psi_r}. \end{aligned} \quad (24)$$

The impedance control mentioned above enables the end effector to track the desired trajectory. However, sometimes, the end effector needs to exert a specified force on the environment, which indicates that the end effector should have the ability to track the desired force. This can implement based on (17) and a force error rather than the interaction force is applied to the impedance model. Then, the desired impedance model and the position correction of the end effector can be reformulated as

$$\begin{aligned} \mathbf{M}_d(\ddot{\mathbf{X}}_d - \ddot{\mathbf{X}}) + \mathbf{B}_d(\dot{\mathbf{X}}_d - \dot{\mathbf{X}}) + \mathbf{K}_d(\mathbf{X}_d - \mathbf{X}) &= \mathbf{F}_d - \mathbf{F}_e, \\ \mathbf{e}(s) &= \frac{\mathbf{E}(s)}{\mathbf{M}_d s^2 + \mathbf{B}_d s + \mathbf{K}_d}, \end{aligned} \quad (25)$$

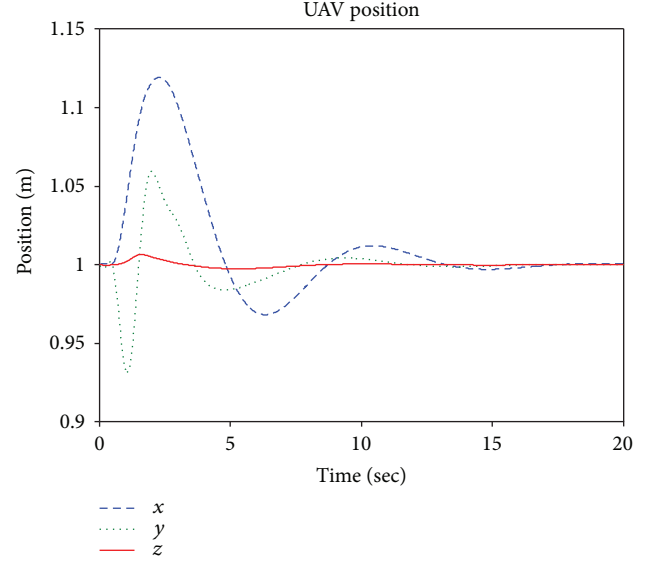


FIGURE 10: Position of the UAV in the inertial frame.

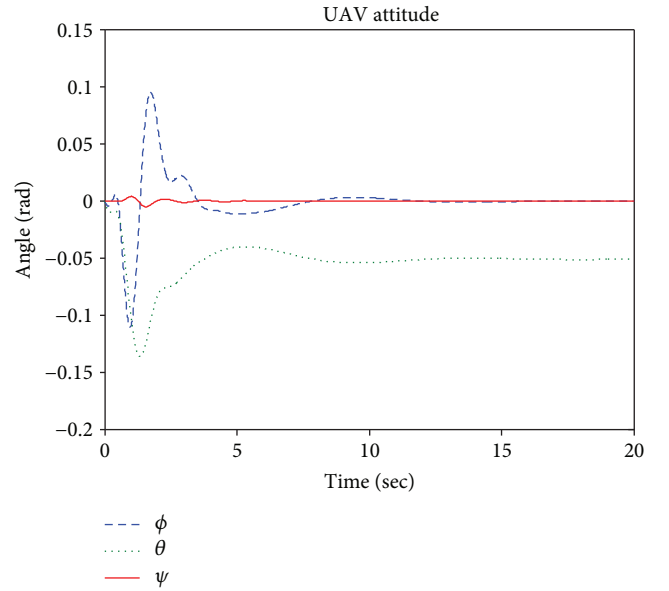


FIGURE 11: Attitude of the UAV.

where  $\mathbf{F}_d$  is the desired force to track and  $\mathbf{E} = \mathbf{F}_d - \mathbf{F}_e$ . Similar to the desired trajectory tracking, the desired force controller can be designed by replacing  $\mathbf{F}_e$  into  $\mathbf{E}$ .

## 5. Simulation

In order to validate the effectiveness of the controller, several simulations have been carried out in the MATLAB/Simulink environment. The purpose of the simulation is that when the quadrotor hovers at a specified point, the manipulator makes contact with a surface. Two cases are studied, that is, the desired trajectory tracking and the desired force tracking. For simplicity, we ignore friction and consider that interaction force is applied to only one direction. Reference position

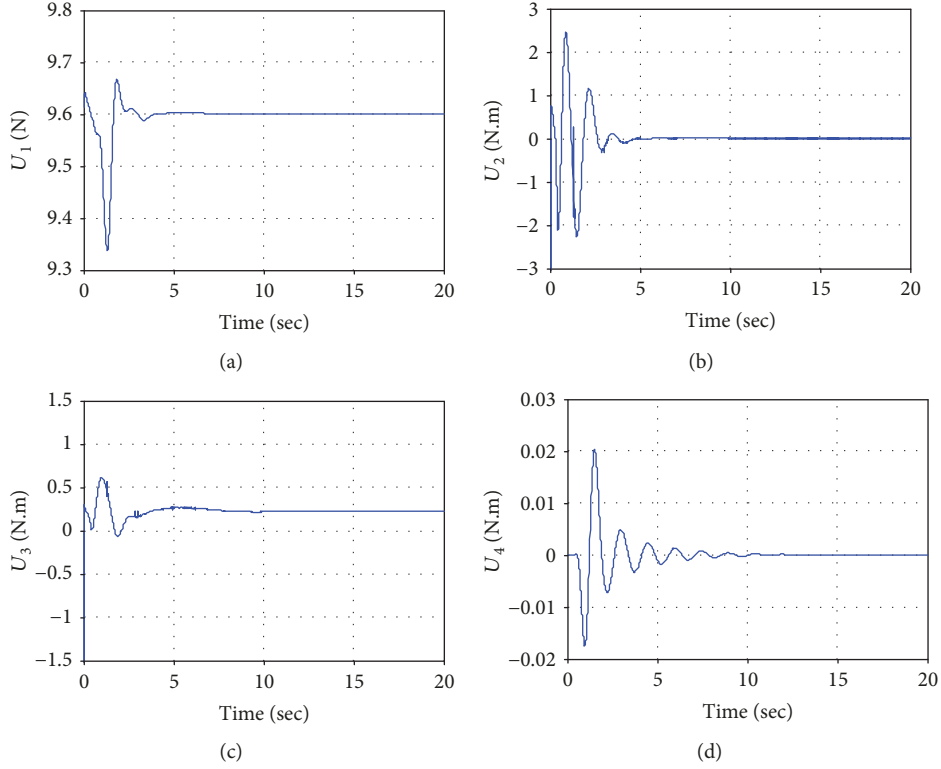


FIGURE 12: Thrust of the UAV.

of the manipulator is set at  $x_{er} = 0.1$  m and a surface is located at  $x_{env} = 0.09$  m with respect to  $\Sigma_b$ . With the given reference position of the end effector, reference joint angle  $a_r$  of the manipulator can be calculated via the inverse kinematics algorithm, and the value of  $a_r$  is  $\pi/6$ . Besides these, the stiffness of the environment  $k_e$  is 100.  $M_d$ ,  $B_d$ , and  $K_d$  are 1, 50, and 625, respectively. The initial condition of the simulation is set to  $\mathbf{q} = [0, 0, 0, 1, 1, 1, 0]^T$ . Simulation adopts variable step. The solver is ODE45 and simulation time is 20 seconds. The involved system parameters values are given in Table 1.

**5.1. Desired Trajectory Tracking.** Simulation results of the end effector during the transition from free motion to interaction are shown below. The quadrotor UAV firstly flies to a position of  $\mathbf{p}_u = (1, 1, 1)$  with respect to  $\Sigma$ , after which it hovers over this point and then the manipulator with an initial joint angle value of 0 approaches the wall and makes contact with it until the end effector arrives at the desired position.

Simulation results of the UAV are shown in Figures 10–12. When the quadrotor hovers at the point  $\mathbf{p}_u$ , the manipulator operates, which results in a quadrotor oscillation. The quadrotor tends to stabilize after the controller works, but the coupling caused by the manipulator leads to a slight tilt of the quadrotor in the pitch angle (shown in Figure 11) and the pitch control torque  $U_3$  (shown in Figure 12) is no long 0. The tilt can allow the UAV to generate a force to offset the contact force. Figure 10 shows that the UAV translation in the  $x$ -axis is obviously affected due to the influence of the UAV pitch motion. The manipulator movements and interaction between the end effector and the surface affect the

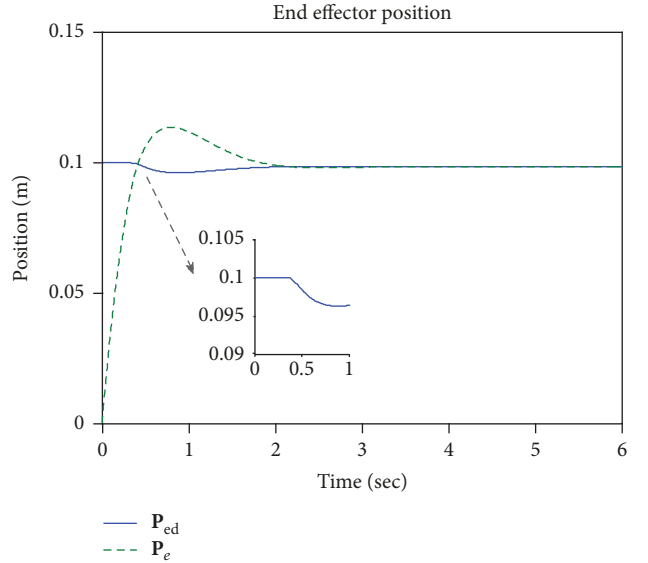


FIGURE 13: Desired and actual position of the end effector in the body frame.

ability of the system, and the control force or torques change so that the UAV can return to a stable state quickly.

Figures 13–16 shows the simulation of the end effector. From 0 to about 0.4 seconds, the manipulator moves in the free space, and the interaction force is 0 (shown in Figure 15), which results in a position correction value of 0 and the reference position is equal to the desired position during this time period (shown in Figure 13). After 0.4

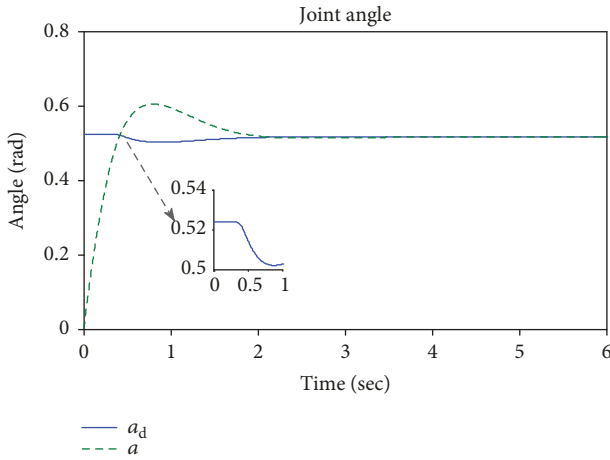


FIGURE 14: Desired and actual joint angle of the manipulator.

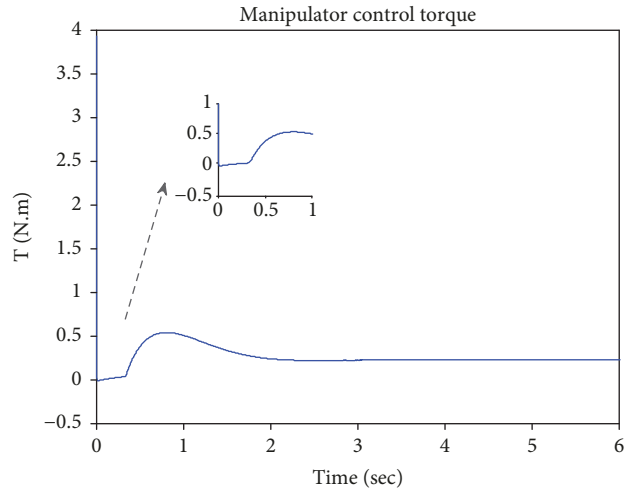


FIGURE 16: Joint torque for the manipulator.

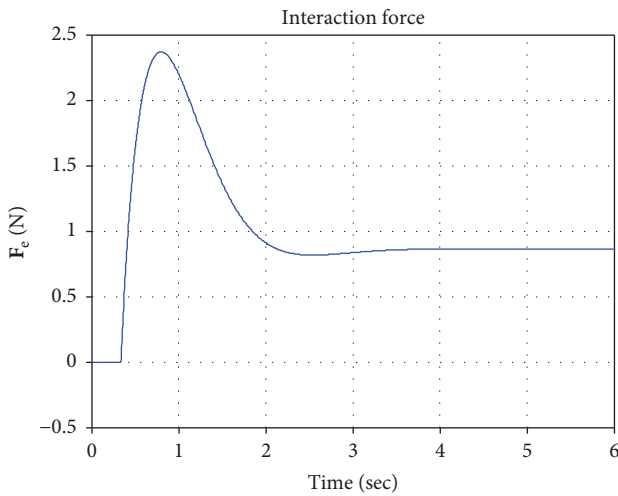


FIGURE 15: Interaction force between the end effector and the surface.

seconds, the end effector contacts the surface, and the interaction force is no longer 0. Figure 15 shows that when the end effector makes contact with the surface at a certain speed, the interaction may keep growing due to inertia, then the impedance controller works so that the interaction force and the end effector position meet the desired dynamic relationship. Figure 13 shows that the desired position of the end effector is less than the given reference value 0.1, which can be explained by the fact that when the desired dynamic relationship mentioned above meets the requirements, the end effector reaches a proper position to avoid an excessive contact force. This is why the impedance control can reduce the damage of the end effector and the interactive objects.

**5.2. Desired Force Tracking.** The desired force  $F_d$  is 1 N, and other simulation conditions are the same as the desired trajectory tracking simulation. Simulation results of the UAV are shown in Figures 17–23. Similar to the desired trajectory tracking, the UAV hovers at a position of  $\mathbf{p}_u = (1, 1, 1)$  with respect to  $\Sigma$ . Figure 17 shows that the UAV flies in a

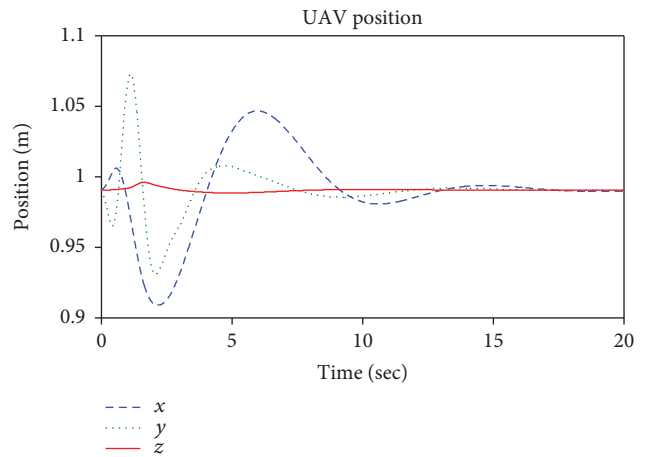


FIGURE 17: Position of the UAV in the inertial frame.

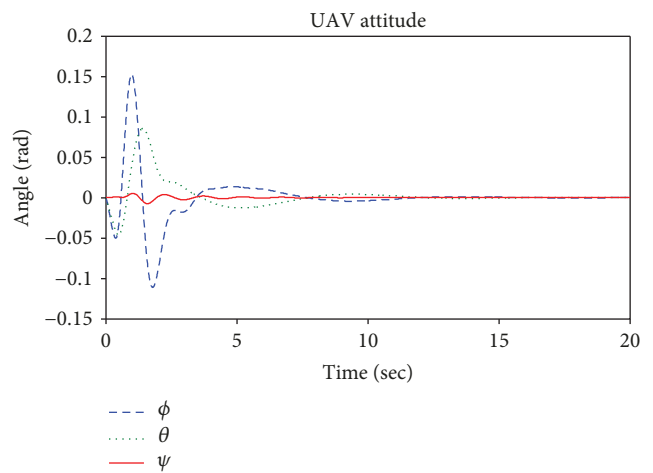


FIGURE 18: Attitude of the UAV.

neighborhood of point  $\mathbf{p}_u$  and after about 13 seconds, the UAV tends to hovers although there is still a tiny error. Compared with Figure 11, Figure 18 reflects a better convergence

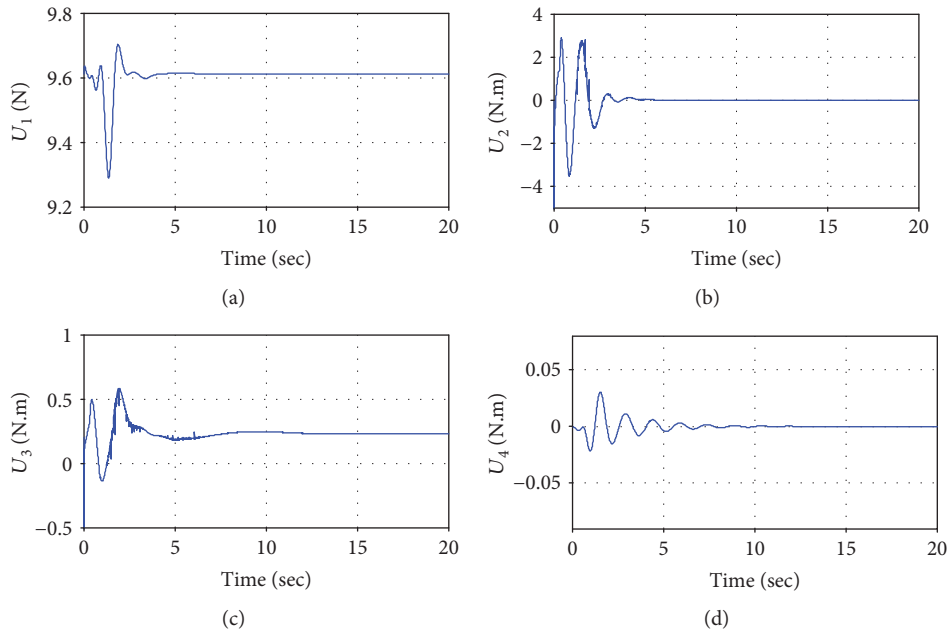


FIGURE 19: Thrust of the UAV.

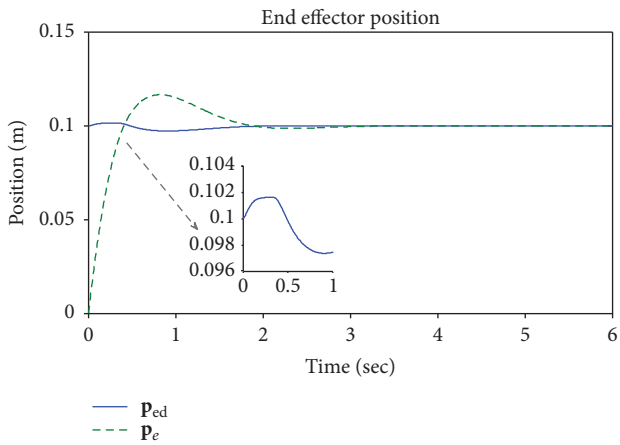


FIGURE 20: Desired and actual position of the end effector in the body frame.

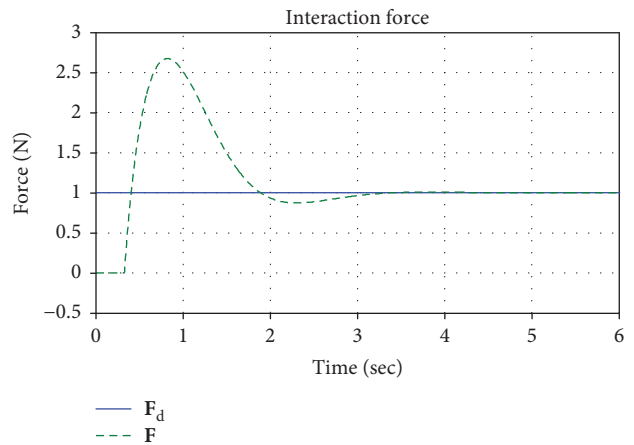


FIGURE 22: Interaction force between the end effector and the surface.

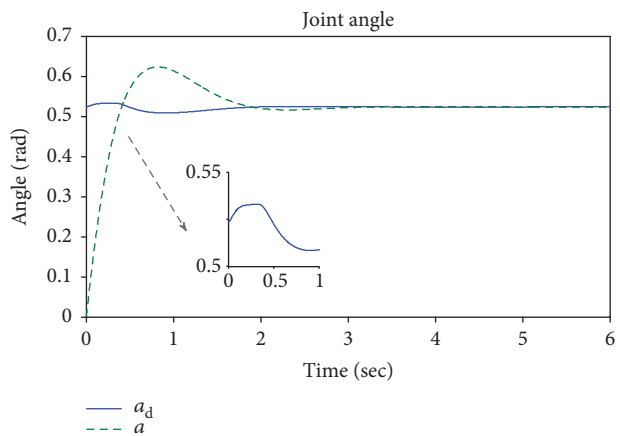


FIGURE 21: Desired and actual joint angle of the manipulator.

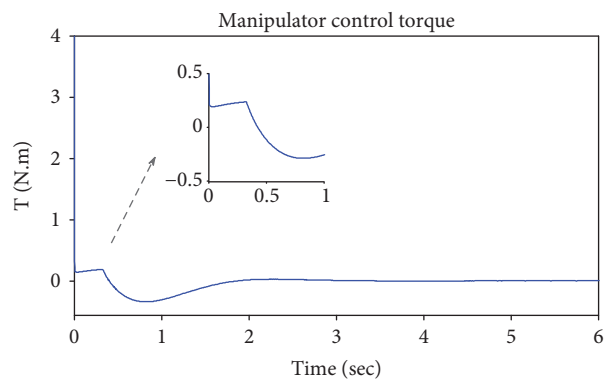


FIGURE 23: Joint torque for the manipulator.

effect especially the case of pitch angle and it reaches 0 despite the presence of interaction between the end effector and the environment. This is mainly because the given desired force  $F_d$ , which may be thought to offset the interaction force. Both simulations of the desired trajectory tracking and the force tracking indicate that the manipulator movements and the environment contacts have an impact on the UAV stability; however, the height and yaw motion suffer a relatively little impact. From Figure 19, due to the manipulator influence, it is can be seen that the UAV pitch control torque  $U_3$  is not 0 although the pitch angle can reach 0 after the controller works.

Figures 20–23 shows the simulation results of the end effector. From 0 to about 0.4 seconds, the manipulator moves in the free space, and the interaction force is 0, as shown in Figure 22. However, different from Figures 13 and 14, Figures 20 and 21 show that the desired position and joint angle of the manipulator changes during the movements in the free space. This can be explained by the desired impedance model (25), and position correction is not 0 due to the given desired force. After about 0.4 seconds, the controller works, and it tracks the desired force perfectly and the tracking error is 0, which results in a position correction value of 0 and the reference position is equal to the desired position. The joint control torque slightly increases to make the end effector reach the surface. Different from Figure 16, the joint torque decreases as the interaction force increases, as shown in Figure 23 and when the system gets stable, the torque remains a fixed value.

## 6. Conclusion

This paper has presented the model and the dynamic stability analysis of a manipulating unmanned aerial vehicle, and numerical simulation is used to test the work. The system modeling based on Euler-Poincare equation is simple and efficient by means of computer symbol derivation. Lyapunov exponent method used to analyze the dynamic stability just considering the manipulator movements has shown obvious advantages. It is constructive and simple for the exponent calculation when compared with Lyapunov's stability theory. Simulation results illustrate that the coupling between the manipulator and the quadrotor will affect the dynamic stability of the MUAV, and the coupling compensation can reduce the influence. As for interaction dynamic stability, the proposed impedance controller is shown to be able to stabilize the system both in the free flight and in the presence of interaction.

## Conflicts of Interest

The authors declare that they have no conflicts of interest.

## Acknowledgments

The authors thank the anonymous reviewers for helpful and insightful remarks. Helpful discussions with Professor Wu Qiong on her guidance in Lyapunov exponent theory are gratefully acknowledged. This research is supported by the

National Natural Science Foundation of China (51405243 and 51575283).

## References

- [1] K. Nonami, "Prospect and recent research & development for civil use autonomous unmanned aircraft as UAV and MAV," *Journal of System Design and Dynamics*, vol. 1, no. 2, pp. 120–128, 2007.
- [2] K. Herrick, "Development of the unmanned aerial vehicle market: forecasts and trends," *Air & Space Europe*, vol. 2, no. 2, pp. 25–27, 2000.
- [3] V. Ghadiok, J. Goldin, and W. Ren, "Autonomous indoor aerial gripping using a quadrotor," in *2011 IEEE/RSJ International Conference on Robotics and Systems (IROS)*, pp. 4645–4651, San Francisco, CA, USA, September 2011.
- [4] D. Mellinger, Q. Lindsey, M. Shomin, and V. Kumar, "Design, modeling, estimation and control for aerial grasping and manipulation," in *2011 IEEE/RSJ International Conference on Intelligent Robots and Systems (IROS)*, pp. 2668–2673, San Francisco, CA, USA, September 2011.
- [5] P. E. I. Pounds, D. R. Bersak, and A. M. Dollar, "Grasping from the air: hovering capture and load stability," in *2011 IEEE International Conference on Robotics and Automation (ICRA)*, pp. 2491–2498, Shanghai, China, May 2011.
- [6] S. Kim, H. Seo, S. Choi, and H. J. Kim, "Vision-guided aerial manipulation using a multirotor with a robotic arm," *IEEE/ASME Transactions on Mechatronics*, vol. 21, no. 4, pp. 1912–1923, 2016.
- [7] R. Mebarki and V. Lippiello, "Image-based control for aerial manipulation," *Asian Journal of Control*, vol. 16, no. 3, pp. 646–656, 2014.
- [8] T. W. Danko and P. Y. Oh, "Design and control of a hyper-redundant manipulator for mobile manipulating unmanned aerial vehicles," *Journal of Intelligent & Robotic Systems*, vol. 73, no. 1-4, pp. 709–723, 2014.
- [9] J. Mendoza-Mendoza, G. Sepulveda-Cervantes, C. Aguilar-Ibanez et al., "Air-arm: a new kind of flying manipulator," in *2015 Workshop on Research, Education and Development of Unmanned Aerial Systems (RED-UAS)*, pp. 278–287, Cancun, Mexico, November 2015.
- [10] V. Lippiello and F. Ruggiero, "Exploiting redundancy in Cartesian impedance control of UAVs equipped with a robotic arm," in *2012 IEEE/RSJ International Conference on Intelligent Robots and Systems (IROS)*, pp. 3768–3773, Vilamoura, Portugal, October 2012.
- [11] K. Kondak, F. Huber, M. Schwarzbach et al., "Aerial manipulation robot composed of an autonomous helicopter and a 7 degrees of freedom industrial manipulator," in *2014 IEEE International Conference on Robotics and Automation (ICRA)*, pp. 2107–2112, Hong Kong, China, May-June 2014.
- [12] P. E. I. Pounds, D. R. Bersak, and A. M. Dollar, "Stability of small-scale UAV helicopters and quadrotors with added payload mass under PID control," *Autonomous Robots*, vol. 33, no. 1-2, pp. 129–142, 2012.
- [13] B. Yang, Y. He, J. Han, and G. Liu, "Modeling and control of rotor-flying multi-joint manipulator," *IFAC Proceedings Volumes*, vol. 47, no. 3, pp. 11024–11029, 2014.
- [14] J. Escareno, M. Rakotondrabe, G. Flores, and R. Lozano, "Rotorcraft MAV having an onboard manipulator:

- longitudinal modeling and robust control,” in *2013 European Control Conference (ECC)*, pp. 258–3263, Zurich, Switzerland, July 2013.
- [15] F. Caccavale, G. Giglio, G. Muscio, and F. Pierri, “Adaptive control for UAVs equipped with a robotic arm,” *IFAC Proceedings Volumes*, vol. 47, no. 3, pp. 11049–11054, 2014.
- [16] M. Fumagalli, R. Naldi, A. Macchelli, R. Carloni, S. Stramigioli, and L. Marconi, “Modeling and control of a flying robot for contact inspection,” in *2012 IEEE/RSJ International Conference on Intelligent Robots and Systems (IROS)*, pp. 3532–3537, Vilamoura, Portugal, October 2012.
- [17] M. Orsag, C. Korpela, and P. Oh, “Modeling and control of MM-UAV: mobile manipulating unmanned aerial vehicle,” *Journal of Intelligent & Robotic Systems*, vol. 69, no. 1–4, pp. 227–240, 2013.
- [18] S. Kannan, M. A. Olivares-Mendez, and H. Voos, “Modeling and control of aerial manipulation vehicle with visual sensor,” *IFAC Proceedings Volumes*, vol. 46, no. 30, pp. 303–309, 2013.
- [19] M. Orsag, C. Korpela, S. Bogdan, and P. Oh, “Lyapunov based model reference adaptive control for aerial manipulation,” in *2013 International Conference on Unmanned Aircraft Systems (ICUAS)*, pp. 966–973, Atlanta, GA, USA, May 2013.
- [20] P. Xu, R. Huang, D. Lee, and T. Burg, “Dynamics and control of a novel manipulator on VTOL aircraft (MOVA) system - a planar case study,” in *2014 American Control Conference (ACC)*, pp. 3071–3076, Portland, OR, USA, June 2014.
- [21] M. Kobilarov, “Nonlinear trajectory control of multi-body aerial manipulators,” *Journal of Intelligent & Robotic Systems*, vol. 73, no. 1–4, pp. 679–692, 2014.
- [22] J. Awrejcewicz and G. Kudra, “Stability analysis and Lyapunov exponents of a multi-body mechanical system with rigid unilateral constraints,” *Nonlinear Analysis Theory Methods & Applications*, vol. 63, no. 5–7, pp. e909–e918, 2005.
- [23] Y. Sun, X. Wang, Q. Wu, and N. Sepehri, “On stability analysis via Lyapunov exponents calculated based on radial basis function networks,” *International Journal of Control*, vol. 84, no. 8, pp. 1326–1341, 2011.
- [24] C. Yang, C. Q. Wu, and P. Zhang, “Estimation of Lyapunov exponents from a time series for n -dimensional state space using nonlinear mapping,” *Nonlinear Dynamics*, vol. 69, no. 4, pp. 1493–1507, 2012.
- [25] C. Yang and Q. Wu, “On stabilization of bipedal robots during disturbed standing using the concept of Lyapunov exponents,” in *2006 American Control Conference*, pp. 621–624, Minneapolis, MN, USA, June 2006.
- [26] Y. Sun and C. Q. Wu, “Stability analysis via the concept of Lyapunov exponents: a case study in optimal controlled biped standing,” *International Journal of Control*, vol. 85, no. 12, pp. 1952–1966, 2012.
- [27] E. N. Abdulwahab, Q. A. Atiyah, and A. T. A. Alzahra, “Air-craft lateral-directional stability in critical cases via Lyapunov exponent criterion,” *Al-Khawarizmi Engineering Journal*, vol. 1, no. 9, pp. 29–38, 2013.
- [28] Y. Liu, C. Chen, H. Wu, Y. Zhang, and P. Mei, “Structural stability analysis and optimization of the quadrotor unmanned aerial vehicles via the concept of Lyapunov exponents,” *The International Journal of Advanced Manufacturing Technology*, vol. 94, no. 9–12, pp. 3217–3227, 2018.
- [29] T. Bartelds, A. Capra, S. Hamaza, S. Stramigioli, and M. Fumagalli, “Compliant aerial manipulators: toward a new generation of aerial robotic workers,” *IEEE Robotics and Automation Letters*, vol. 1, no. 1, pp. 477–483, 2016.
- [30] K. Alexis, G. Darivianakis, M. Burri, and R. Siegwart, “Aerial robotic contact-based inspection: planning and control,” *Autonomous Robots*, vol. 40, no. 4, pp. 631–655, 2016.
- [31] F. Forte, R. Naldi, A. Macchelli, and L. Marconi, “Impedance control of an aerial manipulator,” in *2012 American Control Conference (ACC)*, pp. 3839–3844, Montreal, QC, Canada, June 2012.
- [32] H. G. Kwatny and G. L. Blankenship, “Symbolic construction of models for multibody dynamics,” *IEEE Transactions on Robotics and Automation*, vol. 11, no. 2, pp. 271–281, 1995.
- [33] W. C. Zhang, “Chaotic forecasting of natural circulation flow instabilities under rolling motion based on Lyapunov exponents,” *Acta Physica Sinica*, vol. 62, no. 6, pp. 675–675, 2013.
- [34] F. Aghili, “Optimal control of a space manipulator for detumbling of a target satellite,” in *2009 IEEE International Conference on Robotics and Automation*, pp. 362–367, Kobe, Japan, June 2009.
- [35] J. Y. S. Luh, M. W. Walker, and R. P. C. Paul, “On-line computational scheme for mechanical manipulators,” *Journal of Dynamic Systems, Measurement, and Control*, vol. 102, no. 2, pp. 69–76, 1980.
- [36] N. Hogan, “Impedance control of industrial robots,” *Robotics and Computer-Integrated Manufacturing*, vol. 1, no. 1, pp. 97–113, 1984.
- [37] G. Arleo, F. Caccavale, G. Muscio, and F. Pierri, “Control of quadrotor aerial vehicles equipped with a robotic arm,” in *2013 21st Mediterranean Conference on Control & Automation (MED)*, pp. 1174–1180, Chania, Greece, June 2013.



**Hindawi**

Submit your manuscripts at  
[www.hindawi.com](http://www.hindawi.com)

